

# Lightweight Facial Attractiveness Prediction Using Dual Label Distribution

Shu Liu, *Member, IEEE*, Enquan Huang, Ziyu Zhou, Yan Xu, Xiaoyan Kui,  
Tao Lei, *Senior Member, IEEE*, Hongying Meng, *Senior Member, IEEE*

**Abstract**—Facial attractiveness prediction (FAP) aims to assess facial attractiveness automatically based on human aesthetic perception. Previous methods using deep convolutional neural networks have improved the performance, but their large-scale models have led to a deficiency in flexibility. In addition, most methods fail to take full advantage of the dataset. In this paper, we present a novel end-to-end FAP approach that integrates dual label distribution and lightweight design. The manual ratings, attractiveness score, and standard deviation are aggregated explicitly to construct a dual-label distribution to make the best use of the dataset, including the attractiveness distribution and the rating distribution. Such distributions, as well as the attractiveness score, are optimized under a joint learning framework based on the label distribution learning (LDL) paradigm. The data processing is simplified to a minimum for a lightweight design, and MobileNetV2 is selected as our backbone. Extensive experiments are conducted on two benchmark datasets, where our approach achieves promising results and succeeds in balancing performance and efficiency. Ablation studies demonstrate that our delicately designed learning modules are indispensable and correlated. Additionally, the visualization indicates that our approach can perceive facial attractiveness and capture attractive facial regions to facilitate semantic predictions. The code is available at [https://github.com/enquan/2D\\_FAP](https://github.com/enquan/2D_FAP).

**Index Terms**—Facial attractiveness prediction, dual label distribution, lightweight, label distribution learning

## I. INTRODUCTION

**F**ACIAL attractiveness plays a significant role in daily life [1], [2]. It is a complex and multifactorial concept, devoting researchers from diverse disciplines to decrypting its mysteries [3]. Two views from the social sciences have been debated. One is the long-term belief that beauty is in the eye of the beholder, indicating the culture-bound and personalized properties of facial attractiveness. The other is the common notion of general consensus in beauty judgments

This work was supported by the National Natural Science Foundation of China under Grants U22A2034, 62177047 and 62271296, Hunan Provincial Natural Science Foundation of China under Grant 2023JJ30700, and Central South University Research Programme of Advanced Interdisciplinary Studies under Grant 2023QYJC020. We are grateful for resources from the High Performance Computing Center of Central South University.

Shu Liu, Enquan Huang, Ziyu Zhou, Yan Xu, and Xiaoyan Kui are with the School of Computer Science and Engineering, Central South University, Changsha 410083, Hunan, China (e-mail: {sliu35, enquan, zzyotl, taylor\_xy0827, xykui}@csu.edu.cn).

Tao Lei is with the School of Electronic Information and Artificial Intelligence, Shaanxi University of Science and Technology, Xi'an 710021, Shaanxi, China (e-mail: leitao@sust.edu.cn).

Hongying Meng is with the Department of Electronic and Electrical Engineering, Brunel University London, Uxbridge UB8 3PH, UK (e-mail: hongying.meng@brunel.ac.uk).

among observers, indicating its universal human preference. Although the controversy of subjectivity and universality in aesthetic perception has not been settled, these findings form the cognitive basis for facial attractiveness research in computer science [4]. Facial attractiveness prediction (FAP) aims to assess facial attractiveness automatically based on human perception, which facilitates the development of many real-life applications, such as face manipulation and retrieval [5], [6], social media recommendation [7], [8], and cosmetic surgery [9].

In the past two decades, FAP has gradually become a prosperous research topic in computer vision. The methods can be categorized into handcrafted feature based and deep learning based. In most early studies, low-level features like geometric [10], [11] and texture descriptors [12], [13] were manually designed. Such a representation, however, may lack discriminative capability, resulting in poor performance. With the emergence of deep learning, convolutional neural networks (CNNs) [14]–[16] have been applied to FAP. Due to their powerful nonlinearity, CNN-based methods are able to learn hierarchical aesthetic representations thus boosting the performance, but their large-scale models lack flexibility. Adapting neural network architectures to strike a balance between performance and efficiency has been an active research field in recent years. Unfortunately, the lightweight design of FAP has received little attention. The only work utilizing lightweight backbone is to employ MobileNetV2 with co-attention learning mechanism [17].

The FAP datasets usually include facial images with their corresponding manual ratings, ground-truth scores, and standard deviations. Therefore, among CNN-based methods, several labeling schemes have been adopted to meet different learning objectives and employ datasets to varying degrees. The single-label (average score) is the most commonly used, but only one type of label is considered, thus imposing strong restrictions on learning. Although the multi-label scheme cannot adapt well to FAP, its variant, label distribution learning (LDL), has been introduced to provide a novel view of attractiveness learning [18]. Human ratings are aggregated into a label distribution, while the ground-truth score and standard deviation are not utilized explicitly. The LDL paradigm, which aims to learn the latent distributions in the dataset, was formally proposed in [19]. Since then, it has been applied to various tasks, such as age estimation [20], emotion distribution recognition [21], and facial landmark detection [22].

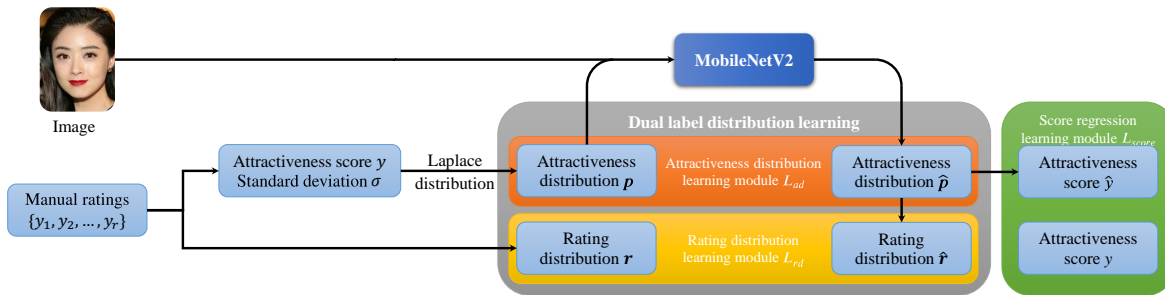


Fig. 1. Overview of our framework. For a given facial image, its manual ratings, attractiveness score, and standard deviation are aggregated explicitly. With the human ratings  $\{y_1, y_2, \dots, y_r\}$ , its attractiveness distribution  $\mathbf{p}$  is generated using the Laplace distribution, while its rating distribution  $\mathbf{r}$  is derived directly. Then, the facial image and  $\mathbf{p}$  are fed into MobileNetV2 to output the predicted attractiveness distribution  $\hat{\mathbf{p}}$ , which is subsequently utilized to compute the predicted attractiveness score  $\hat{y}$  and obtain the predicted rating distribution  $\hat{\mathbf{r}}$ . Finally,  $\hat{\mathbf{p}}$ ,  $\hat{\mathbf{r}}$  and  $\hat{y}$  are jointly optimized under the dual-label distribution and score regression learning modules.

In this paper, we present a novel end-to-end FAP approach consisting of a dual-label distribution and joint learning framework based on lightweight design. The lightweight design lies in many aspects, from data processing to backbone selection. We have simplified the data preprocessing and augmentation to minimum, and conducted extensive experiments to reach the final decision to employ MobileNetV2 as the backbone.

The overview of our framework is shown in Fig. 1. To make the best use of the dataset, the dual-label distribution, including the attractiveness and rating distributions, is proposed and constructed to explicitly utilize the manual ratings, ground-truth score, and standard deviation. Then, it is fed into MobileNetV2 for joint learning, which is designed to optimize three learning modules simultaneously based on the LDL paradigm. The attractiveness distribution learning module aims to optimize the network output, namely, the predicted attractiveness distribution. The rating distribution learning module is designed to refine the predicted rating distribution while further supervising the learning process. The score regression learning module concentrates on further refining the predicted attractiveness score with a novel loss. Finally, given a facial image, the trained model outputs its predicted attractiveness distribution and obtains its attractiveness score to accomplish end-to-end FAP.

The contributions of this paper are summarized as follows.

- We present a novel end-to-end FAP approach that is the first to leverage the lightweight design and LDL paradigm to predict facial attractiveness.
- A dual-label distribution is proposed to take full advantage of the dataset, including the manual ratings, ground-truth score, and standard deviation.
- A joint learning framework is further proposed to optimize the dual-label distribution and concurrently refine the predictions using a novel loss.
- Extensive experiments are conducted on two benchmarks, where our approach achieves appealing results with greatly decreased parameters and computations.

## II. RELATED WORK

### A. Deep Learning Based Facial Attractiveness Prediction

The handcrafted feature based methods advanced the FAP field and achieved some early success. However, such methods

suffer from multiple limitations. First, they are dependent on low-level features that lack representational capability, leading to inferior performance. Second, the model performance relies heavily on feature selection, which the process can be complicated and highly empirical. Third, handcrafted features are strongly constrained because most are based on existing aesthetic criteria or findings from psychological research.

With the emergence of deep learning, numerous CNN-related works have been proposed, many of which have obtained remarkable results on some challenging visual classification or recognition tasks [23], [24]. Meanwhile, the effectiveness of CNNs and their variants has been extensively explored in facial attractiveness prediction. Gray *et al.* were the first to construct a CNN-like hierarchical feedforward model to extract attractiveness features for FAP task [14]. A six-layer CNN was designed to learn the features at multiple levels and directly output the attractiveness score [25]. Later, the VGG network [26] was proposed to extract discriminative deep facial features, which were subsequently utilized for attractiveness prediction [27]. To a certain extent, deeper architectures enable the extraction of more discriminative and representative features.

Simultaneously, researchers have been seeking other paths for enhanced performance and more general solutions. A psychologically inspired CNN (PI-CNN) [28] was proposed for FAP that was fine-tuned with different aesthetic features. Inspired by the effectiveness of facial attributes on facial attractiveness, an attribute-aware CNN (AaNet) [16] was proposed that can integrate attractiveness-related attributes into feature representation to adaptively modulate network filters. Most recently, FAP was redefined as a ranking-guided regression task, where a ranking-guided CNN (R<sup>3</sup>CNN) was constructed to accomplish ranking and regression simultaneously [15]. A two-branch architecture named REX-INCEP was presented in [29]. It employed multiple dynamic loss functions and established an ensemble regressor (CNN-ER) for FAP, which comprises 6 models involving the proposed REX-INCEP. In addition, FAP can be combined with other visual tasks. A hierarchical multitask network that can concurrently determine gender, race, and facial attractiveness of a given portrait image has been designed [30]. Recently, a multitask FAP model was also introduced to automatically predict facial attractiveness

and gender [31].

It is worth noting that FAP research aims to mimic human attractiveness perception, including universal preference shared by a diverse group of observers, and personalized preference of particular individuals. This paper focuses on the universal facial attractiveness prediction, which is also the scope of most existing studies.

### B. Lightweight Architecture

Model efficiency is often a vital indicator in deep learning tasks and is measured by the number of trainable parameters, floating point operations per second (FLOPs), and multiply-adds (MAdds) [32]. In recent years, extensive studies have attempted to adapt neural network architectures to balance between model efficiency and performance, i.e., reducing the amount of model parameters or MAdds while maintaining relatively high performance in multiple tasks, such as SqueezeNet [33], EfficientNet [34], and MobileNet. The MobileNet variants largely depend on separable convolutions to decrease the model size, which decompose standard convolutions into a  $1 \times 1$  pointwise convolution and a depthwise convolution applied to each channel separately. MobileNetV1 [35] is based on a streamlined architecture that uses depthwise separable convolutions. MobileNetV2 [32] utilizes the proposed linear bottleneck with an inverted residual structure. Later, MobileNetV3 [36] was developed through hardware-aware network architecture search, which adopts squeeze and excitation and nonlinearities like swish. Recently, Zhou *et al.* [37] analyzed the disadvantage of the inverted residual block in MobileNetV2, and presented a bottleneck known as the sandglass block. It was then employed to construct MobileNeXt.

The aforementioned lightweight architectures have been broadly employed in multiple tasks, such as popular classification and object detection. A concise self-training method for ImageNet classification was presented, iteratively training smaller and larger EfficientNet models as student and teacher, respectively [38]. A novel family of object detectors named EfficientDet was developed based on EfficientNet backbones and several optimizations for object detection, including a weighted bidirectional feature pyramid network and a compound scaling method [39]. In addition to employing lightweight backbones directly, many researchers have been dedicated to developing models for various tasks based on the lightweight design. The separable convolutions proposed in MobileNets were transferred to construct an efficient graph convolutional network for skeleton-based action recognition [40]. Most recently, the first layer and the first convolutional linear bottleneck of MobileNetV2 were borrowed as feature extractors in a proposed lightweight single-image segmentation network [41].

Although lightweight design has been widely adopted in many tasks, it has been largely ignored in FAP. Only few related studies have been carried out. The prediction of facial attractiveness was enhanced by utilizing pixelwise labeling masks for accurate facial composition and a co-attention learning mechanism with MobileNetV2 [17].

### C. Label Distribution Learning

Previous learning paradigms, such as single-label learning (SLL) and multi-label learning (MLL), address the fundamental question of which label describes the instance. However, neither SLL nor MLL can directly handle further questions with more ambiguity. They are not suitable for some real applications in which the overall distribution of the labels matters. Besides, real-world data with natural measures of label importance exist. Motivated by the above facts, label distribution learning was formally proposed by Geng in 2016 [19], which is a more general learning framework than SLL and MLL. It concentrates on the ambiguity on the label side to learn the latent distribution of the labels. Generally, the label distribution involves a certain number of labels, each describing the importance to the instance.

LDL has been adopted in a wide range of tasks. The emotion distribution learning method was proposed to output the intensity of all basic emotions on a given image [21]. This method addresses the issue of treating the facial expression in an image as only a single emotion. One unified framework with a lightweight architecture was designed to jointly learn age distribution and regress age using the expectation of age distribution [20]. This approach alleviates the high computational cost of large-scale models and the inconsistency between the training and evaluation phases. Motivated by inaccurately annotated landmarks, the soft facial landmark detection algorithm was developed in [22]. It associates each landmark with a bivariate label distribution (BLD), learns the mappings from an image patch to the BLD for each landmark, and finally obtains the facial shape based on the predicted BLDs.

In addition to the aforementioned works, LDL has also been employed in the FAP field. Ren and Geng [42] proposed a beauty distribution transformation to convert  $k$ -wise ratings to label distribution, and a structural LDL method based on structural support vector machine to reveal the human sense of facial attractiveness. Our previous work [18] utilized the inherent score distribution of each image given by human raters as the learning objective and integrated low-level geometric features with high-level CNN features to accomplish automatic attractiveness computation. A deep adaptive LDL framework was developed by Chen and Deng, utilizing discrete label distribution of possible ratings to supervise the FAP learning process [43]. Later, the deep label distribution learning-v2 (DLDL-v2) approach, which originated from age estimation [20], was further designed to estimate facial attractiveness based on the expectation of label distribution through the lightweight ThinAttNet and TinyAttNet [44].

## III. DUAL LABEL DISTRIBUTION

In this section, we present the construction of the dual-label distribution. Some preliminaries are firstly introduced to lay the foundation. Then, the dual-label distribution is proposed in detail, including the rating distribution and the attractiveness distribution, which construct an actual rating distribution and a pseudo rating distribution, respectively. Such distributions are complementary by utilizing the variety of information in the dataset, thus facilitating the network learning.

### A. Preliminaries

1) *The Facial Attractiveness Prediction Problem:* Assume that a training set with  $N$  samples is denoted as  $\{(x^{(i)}, y^{(i)})\}_{i=1}^N$ , where  $x^{(i)}$  and  $y^{(i)}$  denote the  $i$ -th image and its ground-truth score (average score), respectively. We might omit the superscript  $(i)$  for simplicity. The goal of FAP is to learn a mapping from facial images to attractiveness scores such that the error between the predicted score  $\hat{y}$  and ground-truth score  $y$  is as small as possible on an input image  $x$ .

2) *Laplace Distribution:* Both the Laplace distribution and Gaussian distribution are widely used in statistics and data analysis. They share similar symmetry, continuity, and peak location properties. When the variance in the Gaussian distribution approaches infinity, it becomes the Laplace distribution. In this sense, the Laplace distribution can be seen as a more general distribution that includes the Gaussian distribution as a special case. Besides, calculating the probability distribution function for the Laplace distribution is simpler than that for the Gaussian distribution. Therefore, we choose the Laplace distribution in the construction of attractiveness distribution. Defined by the location parameter  $\mu$  and the scale parameter  $b$  (their settings for each image are introduced in Section III-C), the probability density function of the Laplace distribution is

$$f(x|\mu, b) = \frac{1}{2b} \exp\left(-\frac{|x - \mu|}{b}\right) \quad (1)$$

while the cumulative distribution function is

$$F(x|\mu, b) = \frac{1}{2} \left[ 1 + \operatorname{sgn}(x - \mu) \left( 1 - \exp\left(-\frac{|x - \mu|}{b}\right) \right) \right] \quad (2)$$

where the mean and standard deviation of the distribution are  $\mu$  and  $\sqrt{2}b$ , respectively.

During the training phase, the attractiveness distribution is fed into the model, and the rating distribution is employed for supervision. Their generation is introduced in the following.

### B. Rating Distribution

In our previous work [18], a LDL-based FAP method was proposed, which utilized the rating records directly to derive the rating distribution. The ground-truth score and standard deviation, however, were implicitly included, thus ignoring their importance. We follow the same way to construct the rating distribution, represented by the vector  $\mathbf{r}$ .

Let  $r_m$  be the number of raters who rated the image with the attractiveness score  $m$ . Since the attractiveness score is an integer ranging from 1 to 5,  $m = \{1, 2, 3, 4, 5\}$ . Then  $L_1$  normalization is applied to  $\mathbf{r}$  such that  $\sum_{m=1}^5 r_m = 1$ . Thus,  $\mathbf{r}$  represents the actual rating distribution of the image.

### C. Attractiveness Distribution

In order to utilize the ground-truth score  $y$  and the standard deviation  $\sigma$  of the image explicitly, the attractiveness distribution are constructed, which takes advantage of LDL and is represented by the vector  $\mathbf{p}$ .

The formation of  $\mathbf{p}$  is introduced as follows. Each element of  $\mathbf{p}$  represents the probability of the attractiveness score on a certain interval. These probabilities are then combined to

establish the attractiveness distribution. First, we define the interval endpoints  $s_k$

$$s_k = y_{\min} + k \cdot \Delta l \quad (3)$$

where  $y_{\min}$  and  $\Delta l$  are the minimum attractiveness score and interval length, respectively.

Then, the  $j$ -th interval  $I_j$  is formed as

$$I_j = [s_j, s_{j+1}] \quad (4)$$

Its corresponding probability  $p_j$ , namely, the  $j$ -th element of  $\mathbf{p}$ , is calculated using the cumulative distribution function of the Laplace distribution  $F(x|\mu, b)$ .

$$p_j = F(s_{j+1}|\mu, b) - F(s_j|\mu, b) \quad (5)$$

where the location parameter and scale parameter are set to  $\mu = y$  and  $b = \frac{\sigma}{\sqrt{2}}$  for each image, respectively. It is consistent with the mathematical definition, thereby the construction is logical and expected to be viable.

In this work, the interval length  $\Delta l$  is 0.1. To make the best choice of  $\Delta l$ , we have conducted a series of comparative experiments with  $\Delta l = \{0.01, 0.05, 0.1, 0.2, 0.5\}$ , and found that either a larger or smaller  $\Delta l$  would negatively impact the performance. Specifically, with a larger  $\Delta l$ , the model outputs a sparser representation of the attractiveness distribution, which directly decreases its precision and further affects the derived rating distribution. In contrast, with a smaller  $\Delta l$ , the model has to output a distribution with higher dimensions, which is definitely a challenge for lightweight architecture due to its limited representational power.

Since the attractiveness score ranges from 1 to 5 in our adopted datasets,  $s_k$  should share the identical range. Let  $y_{\max}$  and  $y_{\min}$  be the maximum and minimum attractiveness scores, respectively; then,  $y_{\min} = 1$  and  $y_{\max} = 5$ . Note that  $s_k$ ,  $I_j$ , and  $p_j$  are 0-indexed. We have  $k_{\max} = (y_{\max} - y_{\min})/\Delta l = 40$ . Hence, in Eqs. (3)-(5),  $k \in [0, 40]$ ,  $j \in [0, 39]$ .

Finally, we perform an elementwise sigmoid operation and  $L_1$  normalization to  $\mathbf{p}$ . The sigmoid operation offers nonlinear variation to  $\mathbf{p}$ , enhancing its representational power. The  $L_1$  normalization is performed such that  $\sum_{j=0}^{39} p_j = 1$ , hence satisfying the general property of a probability distribution.

## IV. LEARNING

In this section, the employed network architecture and the proposed joint learning framework are introduced in detail.

### A. Network Architecture

Considering the balance between performance and efficiency, MobileNetV2 [32] is selected as our backbone after extensive experiments. As Fig. 2 shows, the building block of MobileNetV2 includes a  $1 \times 1$  expansion convolution and depthwise convolutions followed by a  $1 \times 1$  projection layer. The narrow input and output (bottleneck) are connected with a residual connection. This structure greatly reduces the model size and number of computations while maintaining relatively high performance on multiple tasks. Besides, sigmoid operation and  $L_1$  normalization are also conducted on the output to reduce the inconsistency between the input and output.



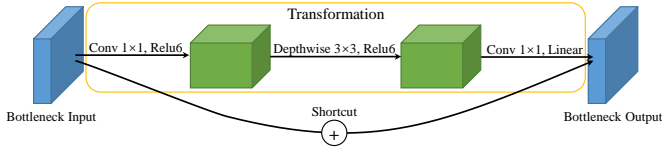


Fig. 2. The building block of MobileNetV2, which consists of linear bottlenecks and an inverted residual structure.

### B. Joint Learning Framework

The joint learning framework contains an attractiveness distribution, a rating distribution and score regression learning modules. As Fig. 1 shows, the input image and its attractiveness distribution are fed into MobileNetV2 to jointly optimize the dual-label distribution and attractiveness score in an end-to-end manner.

1) *Attractiveness Distribution Learning*: The Kullback-Leibler divergence is commonly used in measuring the difference between two probability distributions [18], [20]. However, we adopt the Euclidean distance to measure the similarity between  $\mathbf{p}$  and its prediction  $\hat{\mathbf{p}}$ , whose calculation is much simpler with even better performance. We propose the attractiveness distribution learning module by defining its loss  $L_{ad}$ . The parameter  $n$  in the following equations denotes the number of samples in a minibatch.

$$L_{ad} = \frac{1}{n} \sum_{i=1}^n \|\hat{\mathbf{p}}^{(i)} - \mathbf{p}^{(i)}\|_2 \quad (6)$$

2) *Rating Distribution Learning*: With a single learning module, the proposed approach is unable to perform well due to a lack of model supervision. Therefore, we introduce a rating distribution learning module to reinforce the learning process. The generation of the predicted rating distribution vector  $\hat{\mathbf{r}}$  is described as follows.

Similar to the definition of  $\mathbf{r}$ ,  $\hat{\mathbf{r}}_m$  represents the predicted probability of rating  $m$ , which can be derived from  $\hat{\mathbf{p}}$  using clustering and the rule of rounding. For example, the predicted probability of rating 2 can be computed by  $\hat{\mathbf{p}}$  on the interval [1.5, 2.5). In this sense, we can establish a mapping among the score intervals, ratings, and subscripts in  $\hat{\mathbf{p}}$ , as shown in Table I. Thus,  $\hat{\mathbf{r}}_m$  is defined as

$$\hat{\mathbf{r}}_m = \sum \hat{p}_j, j \in \begin{cases} [0, 4], & m = 1 \\ [10m - 15, 10m - 6], & m = 2, 3, 4 \\ [35, 39], & m = 5 \end{cases} \quad (7)$$

With  $\hat{\mathbf{r}}$  and  $\mathbf{r}$ , we can further supervise the training via the rating distribution loss  $L_{rd}$ . Once again, the Euclidean distance is used to measure the similarity.

$$L_{rd} = \frac{1}{n} \sum_{i=1}^n \|\hat{\mathbf{r}}^{(i)} - \mathbf{r}^{(i)}\|_2 \quad (8)$$

3) *Score Regression Learning*: The above two modules can learn dual-label distribution but fail to account for the attractiveness score. Besides, inconsistency still exists between the training and evaluation stages. Therefore, it is natural

TABLE I  
THE MAPPING AMONG THE SCORE INTERVALS, RATINGS, AND SUBSCRIPTS IN  $\hat{\mathbf{p}}$ .

Score interval	Rating	Subscript in $\hat{\mathbf{p}}$
[1.0, 1.5)	1	[0, 4]
[1.5, 2.5)	2	[5, 14]
[2.5, 3.5)	3	[15, 24]
[3.5, 4.5)	4	[25, 34]
[4.5, 5.0]	5	[35, 39]

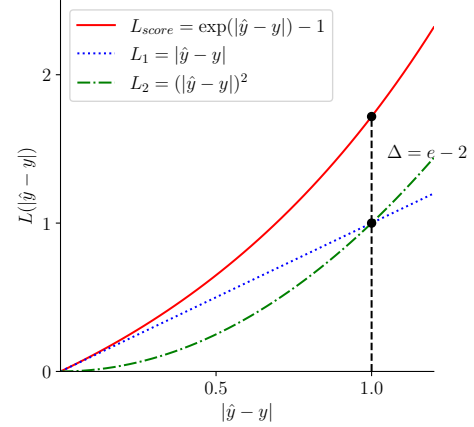


Fig. 3. Comparison of the proposed  $L_{score}$  and  $L_1$ ,  $L_2$  loss. When the absolute error between the ground-truth and predicted score reaches 1,  $L_{score}$  is  $e - 2$  larger than  $L_1$  or  $L_2$  loss, thus refining the score prediction more vigorously.

to incorporate a score regression learning module to further advance the prediction.

The attractiveness score is regressed by

$$\hat{y}^{(i)} = \sum_{j=0}^{39} w_j \hat{p}_j^{(i)} \quad (9)$$

where  $w_j$  is the midpoint of the score interval  $[s_j, s_{j+1}]$  in  $\hat{\mathbf{p}}$ , i.e.,  $w_j = \frac{1}{2}(s_j + s_{j+1})$ . The score regression is similar to the calculation of expectation, when  $w_j$  and  $p_j$  are seen as the weight and probability, respectively.

The score regression loss  $L_{score}$  is then defined in Eq. (10). It is a combination of  $e^v - 1$  and  $L_1$  loss, which is inspired by an important equivalent infinitesimal  $e^v - 1 \sim v(v \rightarrow 0)$ . Thus,  $v$  is replaced by  $e^v - 1$ . As shown in Fig. 3, due to the property of exponential explosion,  $L_{score}$  is much more sensitive to the difference between  $\hat{y}$  and  $y$  than  $L_1$  or  $L_2$  loss. The experiments also demonstrate such superiority.

$$L_{score} = \sum_{i=1}^n [\exp(|\hat{y}^{(i)} - y^{(i)}|) - 1] \quad (10)$$

4) *Joint Loss*: The learning goal of our framework is to find the parameters by jointly learning the attractiveness distribution, rating distribution and score regression, so as to minimize the joint loss  $L$ .

$$L = \lambda_1 L_{ad} + \lambda_2 L_{rd} + \lambda_3 L_{score} \quad (11)$$

where  $\lambda_1$ ,  $\lambda_2$  and  $\lambda_3$  are weights balancing the significance among the three types of losses.

Ablation studies with various combinations of  $\lambda_i = \{1, 2, 5, 10\}$  ( $i = 1, 2, 3$ ) have been performed. Intuitively, we expect the model with higher-weighted  $\lambda_3$  to perform better because our task is to predict the attractiveness score, and the model should focus more on the score regression module. Surprisingly and coincidentally, the model with weights all set to 1 has the best overall performance; thus,  $\lambda_1 = \lambda_2 = \lambda_3 = 1$  in our experiments.

## V. EXPERIMENTS

In this section, we present the experiments to validate the effectiveness of the proposed approach on two benchmark datasets. The implementation details, and comparisons with state-of-the-arts are thoroughly analyzed. Afterward, extensive ablation studies and visualization are carried out to further demonstrate the superiority of our approach.

### A. Implementation Details

All the experiments are conducted on the popular deep learning framework PyTorch [45] with an NVIDIA Tesla V100 GPU. To ensure the effectiveness, five-fold cross validation is performed, and the average results are reported.

*a) Datasets:* The SCUT-FBP5500 [46] and SCUT-FBP [25] datasets are used in our experiments. During the development of these datasets, volunteers were asked to rate images with integers ranging from 1 to 5, where the score 5 indicates the most attractive. Each image was then labeled with its average score. The full rating records are also provided, allowing us to construct different label distributions.

*b) Data Preprocessing:* Since the image size of SCUT-FBP dataset varies, we adopt multitask cascaded CNN (MTCNN) [47] for face and facial landmark detection. Then, the faces are aligned to upright based on the detected landmarks and resized to  $350 \times 350$ . No preprocessing is performed on SCUT-FBP5500 dataset. Finally, the images of SCUT-FBP5500 are resized to  $256 \times 256$  and center-cropped to  $224 \times 224$ , while the aligned images of SCUT-FBP are resized to  $224 \times 224$  directly. Before feeding into the network, all resized images are normalized using the mean and standard deviation of the ImageNet dataset [48] for each color channel.

*c) Data Augmentation:* We only perform random horizontal flipping with a probability of  $p = 0.5$  in the training phase. No data augmentation is performed during the inference stage.

*d) Training Details:* We utilize the ImageNet-pretrained model to initialize the network. Then, the number of output channels of the fully-connected layer in the classifier module is modified to 40. The network is optimized by AdamW [49], with  $\beta = (0.9, 0.999)$  and  $\epsilon = 10^{-8}$ . The initial learning rate is 0.001, and it is decreased by a factor of 10 every 30 epochs. Each model is trained for 90 epochs with a batch size of 256.

*e) Inference Details:* During the inference phase, the preprocessed images are fed into the network to evaluate our approach.

*f) Evaluation Metrics:* FAP can be formulated as a regression problem. Hence, the Pearson correlation coefficient (PC), mean absolute error (MAE), and root mean squared error (RMSE) are employed to evaluate the performance of our method, whose formulas are presented in Eq. (12). A higher PC, and lower MAE and RMSE suggest better performance. Besides, the model efficiency is measured by the number of parameters and MAdds [32].

$$\begin{aligned} \text{PC} &= \frac{\sum_{i=1}^N (y^{(i)} - \bar{y})(\hat{y}^{(i)} - \bar{\hat{y}})}{\sqrt{\sum_{i=1}^N (y^{(i)} - \bar{y})^2} \sqrt{\sum_{i=1}^N (\hat{y}^{(i)} - \bar{\hat{y}})^2}} \\ \text{MAE} &= \frac{1}{N} \sum_{i=1}^N |\hat{y}^{(i)} - y^{(i)}| \\ \text{RMSE} &= \sqrt{\frac{1}{N} \sum_{i=1}^N (\hat{y}^{(i)} - y^{(i)})^2} \end{aligned} \quad (12)$$

where  $N$  denotes the number of images in the test set,  $\bar{y} = \frac{1}{N} \sum_{i=1}^N y^{(i)}$ , and  $\bar{\hat{y}} = \frac{1}{N} \sum_{i=1}^N \hat{y}^{(i)}$ .

### B. Comparison with the State of the Art

We compare our approach against several recent and representative works on both datasets. The comparison with state of the art is given in Table II, which proves our advantages in terms of performance and efficiency. Note that all the comparison methods use the code and experimental settings that are publicly available in the original papers.

*1) High performance:* On the SCUT-FBP5500 dataset, our approach achieves state-of-the-art performance on three evaluation metrics, surpassing previous methods utilizing non-lightweight backbones (e.g. ResNets, ResNeXts) [15], [16], [31] by a large margin. The recently proposed CNN-ER [29] adopted a large-scale ensemble model with dynamic loss functions to facilitate the prediction, yet our method performs slightly better. Additionally, when compared with the method using the same backbone [17], ours still performs slightly better. On the SCUT-FBP dataset, our approach yields comparable results. Previous studies tend to adopt complicated data augmentation [16], [18] to seek better performance, while ours abandons such techniques to make them simple and lightweight. As for DLDL-v2 [44], we infer that its superiority largely resulted from pretraining. ThinAttNet was pretrained on the MS-Celeb-1M dataset, a face recognition dataset that is more relevant to our task than the object classification dataset, e.g., the ImageNet dataset. Compared with the most recent R<sup>3</sup>CNN [15], although our approach has a slightly lower PC, its relatively higher MAE and RMSE indicate poorer predictions, which is unacceptable in FAP.

*2) High efficiency:* Our approach has the fewest parameters and MAdds among the compared methods. It is also an extension of our previous work [18], as it significantly improves model efficiency while achieving similar performance on SCUT-FBP. Compared with those using ResNet-18 or ResNet-50/ResNeXt-50, our method has an 80% or 90% reduction in the number of parameters and MAdds, respectively. A majority of previous methods employ deep models to achieve better

TABLE II

COMPARISON WITH THE STATE OF THE ART ON SCUT-FBP5500 AND SCUT-FBP DATASETS. THE BEST RESULTS ARE PRESENTED IN BOLD.

Method on SCUT-FBP5500 dataset	Backbone	#Params(M)	MAdds(G)	PC $\uparrow$	MAE $\downarrow$	RMSE $\downarrow$
AaNet [16]	ResNet-18	11.69	1.82	0.9055	0.2236	0.2954
Co-attention learning [17]	MobileNetV2 $\times 2$	7.00	0.62	0.9260	0.2020	0.2660
MT-ResNet [31]	ResNet-50	25.56	4.11	0.8905	0.2459	0.3208
R <sup>3</sup> CNN [15]	ResNeXt-50	25.03	4.26	0.9142	0.2120	0.2800
CNN-ER [29]	Ensemble of 6 models	255.00	-	0.9250	0.2009	0.2650
Ours	MobileNetV2	<b>2.28</b>	<b>0.31</b>	<b>0.9276</b>	<b>0.1964</b>	<b>0.2585</b>
Method on SCUT-FBP dataset	Backbone	#Params(M)	MAdds(G)	PC $\uparrow$	MAE $\downarrow$	RMSE $\downarrow$
LDL [18]	ResNet-50	25.56	4.11	0.9301	0.2127	0.2781
P-AaNet [16]	ResNet-18	11.69	1.82	0.9103	0.2224	0.2816
DLDL-v2 [44]	ThinAttNet	3.69	3.86	0.9300	<b>0.2120</b>	<b>0.2730</b>
R <sup>3</sup> CNN [15]	ResNeXt-50	25.03	4.26	<b>0.9500</b>	0.2314	0.2885
Ours	MobileNetV2	<b>2.28</b>	<b>0.31</b>	0.9309	0.2212	0.2822

TABLE III

COMPARISON OF DIFFERENT COMBINATIONS OF LEARNING MODULES, WHERE AD, RD, AND SR STAND FOR THE LEARNING OF ATTRACTIVENESS DISTRIBUTION, RATING DISTRIBUTION, AND SCORE REGRESSION, RESPECTIVELY.

Learning module	SCUT-FBP5500			SCUT-FBP		
	PC $\uparrow$	MAE $\downarrow$	RMSE $\downarrow$	PC $\uparrow$	MAE $\downarrow$	RMSE $\downarrow$
AD	0.9147 $\pm$ 0.0053	0.5651 $\pm$ 0.0001	0.6823 $\pm$ 0.0001	0.8168 $\pm$ 0.0263	0.6651 $\pm$ 0.0004	0.7902 $\pm$ 0.0005
AD + RD	0.9243 $\pm$ 0.0020	0.2094 $\pm$ 0.0027	0.2746 $\pm$ 0.0040	0.9169 $\pm$ 0.0047	0.2679 $\pm$ 0.0065	0.3301 $\pm$ 0.0079
AD + SR	0.9272 $\pm$ 0.0015	0.1966 $\pm$ 0.0022	0.2592 $\pm$ 0.0026	0.9271 $\pm$ 0.0042	0.2273 $\pm$ 0.0049	0.2900 $\pm$ 0.0073
AD + RD + SR	<b>0.9276<math>\pm</math>0.0016</b>	<b>0.1964<math>\pm</math>0.0024</b>	<b>0.2585<math>\pm</math>0.0028</b>	<b>0.9309<math>\pm</math>0.0025</b>	<b>0.2212<math>\pm</math>0.0049</b>	<b>0.2822<math>\pm</math>0.0041</b>

performance. We, however, focus on the lightweight design to enable the model to be suitable for resource-constrained circumstances.

Overall, our approach succeeds in striking a balance between performance and efficiency, achieving state-of-the-art or comparable results in both datasets while sharply decreasing the number of parameters and MAdds.

### C. Ablation Study

In order to investigate the effectiveness of each learning module and backbone more precisely, we conduct an extensive ablation study as follows.

1) *Different combinations of learning modules*: To demonstrate that all learning modules are indispensable and internally correlated, different combinations of them are compared in Table III. The models with only attractiveness distribution (AD) learning module perform poorly, with exceedingly high MAE and RMSE, along with a very low PC on the SCUT-FBP dataset. After introducing the rating distribution (RD) or score regression (SR) learning module, the performance significantly improves. Notably, introducing the SR learning module enables the model to perform similarly to the full model, which can be well explained that our task is to predict facial attractiveness in the form of a score. Compared with the rating distribution, the attractiveness score is more relevant to our task. Furthermore, the performance continues to increase when we utilize the full model. Such growth is particularly significant on SCUT-FBP, indicating that smaller datasets benefit more from the RD and SR learning modules.

We can draw some conclusions from the above results. First, all modules are indeed indispensable. The AD learning module is the base, and the other two refine the prediction by introducing related supervised information. To a certain extent, the SR learning module is a must for our task.

Second, the smaller dataset requires more supervision for better performance, and the issue of overfitting simultaneously should be considered. Finally, appropriate supervision is vital for training. The choice of supervision, which avoids internal redundancy, is also important.

2) *Different backbones*: To explore the efficacy of different backbones, we carry out experiments under identical settings on representative backbones, which are categorized as traditional or lightweight. As shown in Table IV, MobileNetV2 has the best overall performance on both datasets, especially on SCUT-FBP, surpassing other backbones by a large margin. For traditional backbones, ResNet-18 has similar results, but the parameters and MAdds increase by 5 times. All evaluation metrics suffer when using deeper variants of ResNet or VGG, notably in SCUT-FBP. We infer that such phenomenon mainly results from overfitting and overtraining. First, there are only 4400 and 400 training samples in two datasets, respectively. Training a very deep model (e.g., ResNet-50) with a small or tiny dataset is prone to overfitting. Second, we notice that models with ResNet-50 or VGG19 have larger training losses than the corresponding ResNet-18 or VGG16, suggesting that the training settings might not be suitable for deeper architectures. Lastly, we adjust the training setup of the ResNet-50 model so that it can be properly trained and achieve improved performance; however, it is still inferior to the model employing MobileNetV2.

For lightweight backbones, we conduct experiments on MobileNetV3 [36]. The formerly proposed MobileNetV2 still enjoys clear superiority. We notice that the performance declines with larger MobileNetV3 on SCUT-FBP, which is consistent with the traditional backbones. Thus, we can conclude that the choice of backbone in terms of scale and structure is significant in performance and requires careful consideration.

TABLE IV  
COMPARISON OF DIFFERENT BACKBONES.

Backbone	#Params(M)	MAdds(G)	SCUT-FBP5500			SCUT-FBP		
			PC $\uparrow$	MAE $\downarrow$	RMSE $\downarrow$	PC $\uparrow$	MAE $\downarrow$	RMSE $\downarrow$
ResNet-18	11.20	1.82	0.9262 $\pm$ 0.0014	0.1961 $\pm$ 0.0020	0.2605 $\pm$ 0.0025	0.9238 $\pm$ 0.0038	0.2295 $\pm$ 0.0070	0.3007 $\pm$ 0.0082
ResNet-50	23.59	4.11	0.9198 $\pm$ 0.0016	0.2058 $\pm$ 0.0023	0.2728 $\pm$ 0.0029	0.9067 $\pm$ 0.0070	0.2591 $\pm$ 0.0090	0.3354 $\pm$ 0.0105
VGG16	14.74	15.39	0.9267 $\pm$ 0.0014	<b>0.1952<math>\pm</math>0.0019</b>	0.2593 $\pm$ 0.0023	0.9164 $\pm$ 0.0040	0.2627 $\pm$ 0.0121	0.3377 $\pm$ 0.0183
VGG19	20.06	19.55	0.9251 $\pm$ 0.0014	0.1978 $\pm$ 0.0021	0.2621 $\pm$ 0.0023	0.9135 $\pm$ 0.0148	0.2719 $\pm$ 0.0258	0.3515 $\pm$ 0.0459
MobileNetV3_large	4.25	0.22	0.9210 $\pm$ 0.0018	0.2025 $\pm$ 0.0022	0.2688 $\pm$ 0.0028	0.9122 $\pm$ 0.0057	0.2776 $\pm$ 0.0106	0.3472 $\pm$ 0.0128
MobileNetV3_small	1.56	0.06	0.9103 $\pm$ 0.0019	0.2142 $\pm$ 0.0023	0.2850 $\pm$ 0.0028	0.9156 $\pm$ 0.0059	0.2631 $\pm$ 0.0099	0.3427 $\pm$ 0.0148
MobileNetV2	2.28	0.31	<b>0.9276<math>\pm</math>0.0016</b>	0.1964 $\pm$ 0.0024	<b>0.2585<math>\pm</math>0.0028</b>	<b>0.9309<math>\pm</math>0.0025</b>	<b>0.2212<math>\pm</math>0.0049</b>	<b>0.2822<math>\pm</math>0.0041</b>

TABLE V  
COMPARISON OF DIFFERENT LDL SCHEMES.

LDL scheme	SCUT-FBP5500			SCUT-FBP		
	PC $\uparrow$	MAE $\downarrow$	RMSE $\downarrow$	PC $\uparrow$	MAE $\downarrow$	RMSE $\downarrow$
[18]	0.9259 $\pm$ 0.0018	0.1965 $\pm$ 0.0026	0.2606 $\pm$ 0.0032	0.9211 $\pm$ 0.0058	0.2283 $\pm$ 0.0095	0.2954 $\pm$ 0.0100
[44]	0.9253 $\pm$ 0.0016	0.2074 $\pm$ 0.0019	0.2722 $\pm$ 0.0024	0.9184 $\pm$ 0.0040	0.2692 $\pm$ 0.0029	0.3439 $\pm$ 0.0042
Ours with Gaussian distribution	0.9275 $\pm$ 0.0014	0.1966 $\pm$ 0.0021	0.2587 $\pm$ 0.0024	0.9263 $\pm$ 0.0040	0.2271 $\pm$ 0.0063	0.2910 $\pm$ 0.0075
Ours with Laplace distribution	<b>0.9276<math>\pm</math>0.0016</b>	<b>0.1964<math>\pm</math>0.0024</b>	<b>0.2585<math>\pm</math>0.0028</b>	<b>0.9309<math>\pm</math>0.0025</b>	<b>0.2212<math>\pm</math>0.0049</b>	<b>0.2822<math>\pm</math>0.0041</b>

3) *Different label distribution learning schemes*: To demonstrate the superiority of our approach among LDL methods, we carry out the following comparative experiments. The approach in [18] is reimplemented on SCUT-FBP5500, since the dataset had not been released at the time of publication of the paper. Then, the method in [20], which was originally designed for age estimation, was adapted to FAP since it is a similar regression task to that used in [44]. For a fair comparison, the methods mentioned above are reimplemented using MobileNetV2 under identical training settings. Furthermore, we compare the performances of the Gaussian and Laplace distributions by replacing the probability distribution employed in the attractiveness distribution. As Table V shows, our delicately designed approach achieves the best performance on both datasets, notably on SCUT-FBP, greatly outperforming the other methods. When comparing Laplace and Gaussian distributions, our approach with the Laplace distribution performs slightly better on SCUT-FBP5500 but significantly better on SCUT-FBP, proving the effectiveness and simplicity of Laplace distribution.

#### D. Visualization

To better understand how our model perceives abstract facial attractiveness, we visualize a feature map that can intuitively present the prediction patterns of different degrees of attractiveness, and indicate the reasons for good or poor predictions.

Here the visualization follows the class activation mapping (CAM) method [50]. The global average pooling (GAP) is applied to the last feature map of the model to calculate the mean of each channel. The results are then mapped to the attractiveness score via the fully-connected layer, and its gradients with respect to the last feature map are calculated. The ReLU6 activation layer in the last convolution block of MobileNetV2 produces  $7 \times 7$  feature maps with 1280 channels. These feature maps are first channel-wise averaged and resized to  $224 \times 224$ . Finally, those gradients are visually presented on the input images, as shown in Fig. 4.

We observe that our approach shows different perception patterns for faces with different levels of attractiveness. When the ground-truth score is low, the approach evaluates the face by looking at the larger facial areas. It is consistent with findings in cognitive neuroscience and clinical psychology, that people tend to devote more attention to full observation of the face before giving a low rating [51], [52]. With an increasing degree of attractiveness, our approach gradually focuses on certain facial regions (e.g., mouth, eyes, nose) and produces semantic predictions. It is consistent with findings that people are easily attracted to delicate features (e.g., sensuous lips, large eyes, high nose), and thus give high scores to faces with such positive characteristics [52], [53].

From good predictions, human-like behavior can be discovered to demonstrate the effectiveness of our approach. In Fig. 4(a), the high-intensity areas almost cover the whole face, indicating that the model fails to locate attractive facial regions, resulting in a relatively low attractiveness score. In Fig. 4(b)(c), the high-intensity areas gradually narrow down to smaller areas, presenting ambiguously semantic predictions. Specifically, when the face is attractive, the model is able to capture abstract facial attractiveness, concentrating on facial regions with evident semantics, such as the eyes and nose in Fig. 4(d). From poor predictions, however, we notice that our approach mainly focuses on irrelevant regions, such as hair, regions outside face, and background, leading to failure in capturing attractiveness, as shown in Fig. 4(e)-(h).

In summary, our approach is capable of sensing facial beauty and capturing attractive facial regions to accomplish accurate and efficient FAP. However, it still has some limitations, mainly due to focusing on irrelevant areas of the images.

#### E. Discussion

Here we highlight five observations from the experiments. Compared with the state-of-the-art works, our method shows advantages in both performance and efficiency. Compared with the traditional single label, our dual label distribution is conducive to improving the FAP performance, especially on



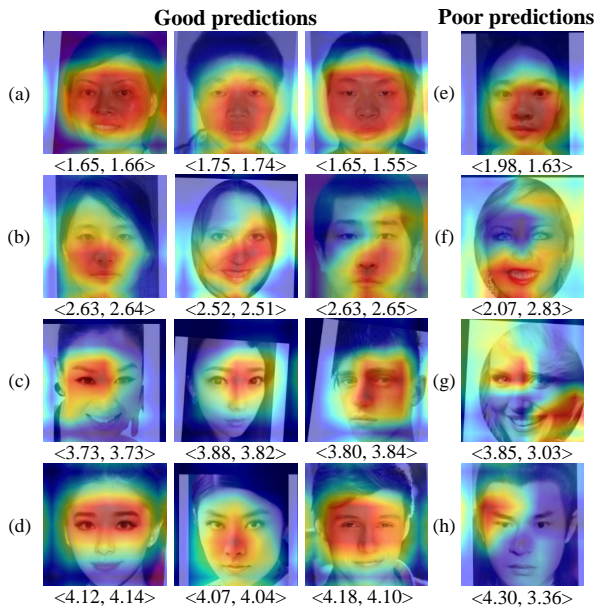


Fig. 4. The heatmap visualization, where warmer colors (e.g., red) indicate higher intensities and cooler colors (e.g., blue) indicate lower intensities. Each row corresponds to a distinct degree of attractiveness. The left three columns ((a)-(d)) and the rightmost column ((e)-(h)) are examples of good and poor predictions, respectively. The pairs below the images represent the  $\langle$ ground-truth score, predicted score $\rangle$ .

smaller-scale datasets. Our well-designed learning modules of attractiveness distribution, rating distribution and score regression play different roles, but they are all indispensable and intrinsically related. Compared with large-scale backbones, lightweight models can reduce the risk of overfitting and perform better on small datasets. By investigating the probability distribution in label distribution construction, the advantages of modeling discrete labels with continuous distribution functions over discrete distributions and using the Laplace distribution in our approach over the Gaussian can be observed.

However, some limitations to our work remain. First, some failure cases exist, where our approach identifies facial features less pertinent to perceived attractiveness, leading to poor predictions. Second, our work is based on static images and fails to consider temporal cues. In fact, psychological [54] and neuroscience [55] studies have proven that temporal cues play a vital role in perceiving facial attractiveness. Nevertheless, little attention has been given to dynamic facial content, and the temporal dynamics of facial attractiveness remain largely unexplored. Kalayci *et al.* [56] utilized dynamic and static features extracted from video clips for facial attractiveness analysis. Recently, Weng *et al.* [57] conducted dynamic facial attractiveness prediction utilizing videos from TikTok. Third, only frontal facial images are employed in our work, which lack variations in visual angles so that fail to reflect the true facial structure. Researchers have shown that facial attractiveness is jointly determined by the frontal view, profile view, and their combination [58]. Therefore, adopting multi-view or three-dimensional facial data for facial attractiveness analysis and prediction, which is expected to produce more comprehensive and reliable results and thus better reveal the

secrets of facial attractiveness, is important. However, such direction has received little attention, and it was not until recently that some researchers started to investigate [59]–[61].

## VI. CONCLUSION

In this paper, we integrate the lightweight design and LDL paradigm to develop a novel facial attractiveness prediction model that consists of (1) a dual-label distribution to take full advantage of the dataset, and (2) a joint learning framework to optimize the dual label distribution and attractiveness score simultaneously. The proposed approach achieves appealing results with greatly decreased parameters and computation. The visualization demonstrates that our approach is interpretable, employing different patterns to capture facial attractiveness so as to generate semantic predictions.

This work has several interesting directions for future exploration. The proposed dual-label distribution is expected to generalize to other similar tasks, such as age prediction and facial expression recognition. For datasets without sufficient information, pseudo distribution can be generated to employ our dual LDL paradigm. In addition, customizing facial attractiveness prediction models is more applicable to person-specific situations, like online dating recommendation. Such personalized prediction leverages previous ratings from a target individual or others with similar preferences to develop a customized model, which is potentially more challenging. The body of related studies is small and the reported accuracy is inferior to universal models.

## REFERENCES

- [1] M. Bashour, "History and current concepts in the analysis of facial attractiveness," *Plastic and Reconstructive Surgery*, vol. 118, no. 3, pp. 741–756, 2006.
- [2] G. Rhodes and J. Haxby, *The Oxford handbook of face perception*. Oxford University Press, 2011.
- [3] M. Ibáñez-Berganza, A. Amico, and V. Loreto, "Subjectivity and complexity of facial attractiveness," *Scientific Reports*, vol. 9, no. 1, p. 8364, 2019.
- [4] S. Liu, Y.-Y. Fan, A. Samal *et al.*, "Advances in computational facial attractiveness methods," *Multimedia Tools and Applications*, vol. 75, no. 23, pp. 16 633–16 663, 2016.
- [5] F. Chen, X. Xiao, and D. Zhang, "Data-driven facial beauty analysis: Prediction, retrieval and manipulation," *IEEE Transactions on Affective Computing*, vol. 9, no. 2, pp. 205–216, 2018.
- [6] X. Ning, S. Xu, F. Nan, Q. Zeng, C. Wang, W. Cai, W. Li, and Y. Jiang, "Face editing based on facial recognition features," *IEEE Transactions on Cognitive and Developmental Systems*, vol. 15, no. 2, pp. 774–783, 2023.
- [7] R. Rothe, R. Timofte, and L. Van Gool, "Some like it hot-visual guidance for preference prediction," in *IEEE Conference on Computer Vision and Pattern Recognition*, 2016, pp. 5553–5561.
- [8] F. S. Abousaleh, W.-H. Cheng, N.-H. Yu, and Y. Tsao, "Multimodal deep learning framework for image popularity prediction on social media," *IEEE Transactions on Cognitive and Developmental Systems*, vol. 13, no. 3, pp. 679–692, 2021.
- [9] A. Bottino, M. De Simone, A. Laurentini *et al.*, "A new 3-d tool for planning plastic surgery," *IEEE Transactions on Biomedical Engineering*, vol. 59, no. 12, pp. 3439–3449, 2012.
- [10] P. Aarabi, D. Hughes, K. Mohajer *et al.*, "The automatic measurement of facial beauty," in *IEEE International Conference on Systems, Man and Cybernetics*, vol. 4, 2001, pp. 2644–2647.
- [11] F. Chen and D. Zhang, "Combining a causal effect criterion for evaluation of facial attractiveness models," *Neurocomputing*, vol. 177, pp. 98–109, 2016.
- [12] A. Kagian, G. Dror, T. Leyvand *et al.*, "A humanlike predictor of facial attractiveness," in *International Conference on Neural Information Processing Systems*, 2006, pp. 649–656.

- [13] D. Zhang, F. Chen, Y. Xu *et al.*, *Computer models for facial beauty analysis*. Springer, 2016.
- [14] D. Gray, K. Yu, W. Xu *et al.*, “Predicting facial beauty without landmarks,” in *European Conference on Computer Vision*, 2010, pp. 434–447.
- [15] L. Lin, L. Liang, and L. Jin, “Regression guided by relative ranking using convolutional neural network (r<sup>3</sup>cnn) for facial beauty prediction,” *IEEE Transactions on Affective Computing*, vol. 13, no. 1, pp. 122–134, 2022.
- [16] L. Lin, L. Liang, L. Jin *et al.*, “Attribute-aware convolutional neural networks for facial beauty prediction,” in *International Joint Conference on Artificial Intelligence*, 2019, pp. 847–853.
- [17] S. Shi, F. Gao, X. Meng *et al.*, “Improving facial attractiveness prediction via co-attention learning,” in *IEEE International Conference on Acoustics, Speech and Signal Processing*, 2019, pp. 4045–4049.
- [18] Y.-Y. Fan, S. Liu, B. Li *et al.*, “Label distribution-based facial attractiveness computation by deep residual learning,” *IEEE Transactions on Multimedia*, vol. 20, no. 8, pp. 2196–2208, 2018.
- [19] X. Geng, “Label distribution learning,” *IEEE Transactions on Knowledge and Data Engineering*, vol. 28, no. 7, pp. 1734–1748, 2016.
- [20] B.-B. Gao, H.-Y. Zhou, J. Wu *et al.*, “Age estimation using expectation of label distribution learning,” in *International Joint Conference on Artificial Intelligence*, 2018, pp. 712–718.
- [21] Y. Zhou, H. Xue, and X. Geng, “Emotion distribution recognition from facial expressions,” in *ACM International Conference on Multimedia*, 2015, pp. 1247–1250.
- [22] K. Su and X. Geng, “Soft facial landmark detection by label distribution learning,” in *AAAI Conference on Artificial Intelligence*, vol. 33, 2019, pp. 5008–5015.
- [23] A. Krizhevsky, I. Sutskever, and G. E. Hinton, “Imagenet classification with deep convolutional neural networks,” *Advances in neural information processing systems*, vol. 25, 2012.
- [24] O. M. Parkhi, A. Vedaldi, and A. Zisserman, “Deep face recognition,” in *British Machine Vision Conference*, 2015.
- [25] D. Xie, L. Liang, L. Jin *et al.*, “Scut-fbp: A benchmark dataset for facial beauty perception,” in *IEEE International Conference on Systems, Man, and Cybernetics*, 2015, pp. 1821–1826.
- [26] K. Simonyan and A. Zisserman, “Very deep convolutional networks for large-scale image recognition,” *arXiv preprint arXiv:1409.1556*, 2014.
- [27] L. Xu, J. Xiang, and X. Yuan, “Transferring rich deep features for facial beauty prediction,” *arXiv preprint arXiv:1803.07253*, 2018.
- [28] J. Xu, L. Jin, L. Liang, Z. Feng, D. Xie, and H. Mao, “Facial attractiveness prediction using psychologically inspired convolutional neural network (pi-cnn),” in *IEEE International Conference on Acoustics, Speech and Signal Processing*, 2017, pp. 1657–1661.
- [29] F. Bougourzi, F. Dornaika, and A. Taleb-Ahmed, “Deep learning based face beauty prediction via dynamic robust losses and ensemble regression,” *Knowledge-Based Systems*, vol. 242, p. 108246, 2022.
- [30] L. Xu, H. Fan, and J. Xiang, “Hierarchical multi-task network for race, gender and facial attractiveness recognition,” in *IEEE International Conference on Image Processing*, 2019, pp. 3861–3865.
- [31] J. Xu, “Mt-resnet: a multi-task deep network for facial attractiveness prediction,” in *IEEE 2nd International Conference on Computing and Data Science*, 2021, pp. 44–48.
- [32] M. Sandler, A. Howard, M. Zhu *et al.*, “Mobilenetv2: Inverted residuals and linear bottlenecks,” in *IEEE Conference on Computer Vision and Pattern Recognition*, 2018, pp. 4510–4520.
- [33] F. N. Iandola, S. Han, M. W. Moskewicz *et al.*, “Squeezenet: Alexnet-level accuracy with 50x fewer parameters and <0.5 mb model size,” *arXiv preprint arXiv:1602.07360*, 2016.
- [34] M. Tan and Q. Le, “Efficientnet: Rethinking model scaling for convolutional neural networks,” in *International Conference on Machine Learning*, 2019, pp. 6105–6114.
- [35] A. G. Howard, M. Zhu, B. Chen *et al.*, “Mobilenets: Efficient convolutional neural networks for mobile vision applications,” *arXiv preprint arXiv:1704.04861*, 2017.
- [36] A. Howard, M. Sandler, G. Chu *et al.*, “Searching for mobilenetv3,” in *IEEE/CVF International Conference on Computer Vision*, 2019, pp. 1314–1324.
- [37] D. Zhou, Q. Hou, Y. Chen, J. Feng, and S. Yan, “Rethinking bottleneck structure for efficient mobile network design,” in *European Conference on Computer Vision*, 2020, pp. 680–697.
- [38] Q. Xie, M.-T. Luong, E. Hovy *et al.*, “Self-training with noisy student improves imagenet classification,” in *IEEE/CVF Conference on Computer Vision and Pattern Recognition*, 2020, pp. 10687–10698.
- [39] M. Tan, R. Pang, and Q. V. Le, “Efficientdet: Scalable and efficient object detection,” in *IEEE/CVF Conference on Computer Vision and Pattern Recognition*, 2020, pp. 10781–10790.
- [40] Y.-F. Song, Z. Zhang, C. Shan, and L. Wang, “Constructing stronger and faster baselines for skeleton-based action recognition,” *IEEE Transactions on Pattern Analysis and Machine Intelligence*, 2022.
- [41] X. Sun, C. Chen, X. Wang, J. Dong, H. Zhou, and S. Chen, “Gaussian dynamic convolution for efficient single-image segmentation,” *IEEE Transactions on Circuits and Systems for Video Technology*, vol. 32, no. 5, pp. 2937–2948, 2022.
- [42] Y. Ren and X. Geng, “Sense beauty by label distribution learning,” in *International Joint Conference on Artificial Intelligence*, 2017, pp. 2648–2654.
- [43] L. Chen and W. Deng, “Facial attractiveness prediction by deep adaptive label distribution learning,” in *Chinese Conference on Biometric Recognition*, 2019, pp. 198–206.
- [44] B.-B. Gao, X.-X. Liu, H.-Y. Zhou, J. Wu, and X. Geng, “Learning expectation of label distribution for facial age and attractiveness estimation,” *arXiv preprint arXiv:2007.01771v2*, 2021.
- [45] A. Paszke, S. Gross, F. Massa *et al.*, “Pytorch: An imperative style, high-performance deep learning library,” in *International Conference on Neural Information Processing Systems*, 2019, pp. 8026–8037.
- [46] L. Liang, L. Lin, L. Jin *et al.*, “Scut-fbp5500: A diverse benchmark dataset for multi-paradigm facial beauty prediction,” in *International Conference on Pattern Recognition*, 2018, pp. 1598–1603.
- [47] K. Zhang, Z. Zhang, Z. Li *et al.*, “Joint face detection and alignment using multitask cascaded convolutional networks,” *IEEE Signal Processing Letters*, vol. 23, no. 10, pp. 1499–1503, 2016.
- [48] J. Deng, W. Dong, R. Socher *et al.*, “Imagenet: A large-scale hierarchical image database,” in *IEEE Conference on Computer Vision and Pattern Recognition*, 2009, pp. 248–255.
- [49] I. Loshchilov and F. Hutter, “Decoupled weight decay regularization,” in *International Conference on Learning Representations*, 2019.
- [50] B. Zhou, A. Khosla, A. Lapedriza, A. Oliva, and A. Torralba, “Learning deep features for discriminative localization,” in *IEEE Conference on Computer Vision and Pattern Recognition*, 2016, pp. 2921–2929.
- [51] H. J. Richards, V. Benson, N. Donnelly, and J. A. Hadwin, “Exploring the function of selective attention and hypervigilance for threat in anxiety,” *Clinical Psychology Review*, vol. 34, no. 1, pp. 1–13, 2014.
- [52] L. Zhu, H. Zhou, X. Wang, X. Ma, and Q. Liu, “Preference for ugly faces? —A cognitive study of attentional and memorial biases toward facial information among young females with facial dissatisfaction,” *Frontiers in Psychology*, vol. 13, p. 1024197, 2022.
- [53] H. Kou, Y. Su, T. Bi, X. Gao, and H. Chen, “Attentional biases toward face-related stimuli among face dissatisfied women: Orienting and maintenance of attention revealed by eye-movement,” *Frontiers in Psychology*, vol. 7, p. 919, 2016.
- [54] A. J. Rubenstein, “Variation in perceived attractiveness: Differences between dynamic and static faces,” *Psychological science*, vol. 16, no. 10, pp. 759–762, 2005.
- [55] A. J. O’Toole, D. A. Roark, and H. Abdi, “Recognizing moving faces: A psychological and neural synthesis,” *Trends in cognitive sciences*, vol. 6, no. 6, pp. 261–266, 2002.
- [56] S. Kalayci, H. K. Ekenel, and H. Gunes, “Automatic analysis of facial attractiveness from video,” in *IEEE International Conference on Image Processing*, 2014, pp. 4191–4195.
- [57] N. Weng, J. Wang, A. Li, and Y. Wang, “Two-stream temporal convolutional network for dynamic facial attractiveness prediction,” in *International Conference on Pattern Recognition*, 2021, pp. 10026–10033.
- [58] Q. Liao, X. Jin, and W. Zeng, “Enhancing the symmetry and proportion of 3d face geometry,” *IEEE transactions on visualization and computer graphics*, vol. 18, no. 10, pp. 1704–1716, 2012.
- [59] S. Liu, Y.-Y. Fan, Z. Guo, A. Samal, and A. Ali, “A landmark-based data-driven approach on 2.5 d facial attractiveness computation,” *Neurocomputing*, vol. 238, pp. 168–178, 2017.
- [60] Q. Xiao, Y. Wu, D. Wang, Y.-L. Yang, and X. Jin, “Beauty3dfacenet: deep geometry and texture fusion for 3d facial attractiveness prediction,” *Computers & Graphics*, vol. 98, pp. 11–18, 2021.
- [61] S. Liu, E. Huang, Y. Xu, K. Wang, and D. K. Jain, “Computation of facial attractiveness from 3d geometry,” *Soft Computing*, vol. 26, no. 19, pp. 10401–10407, 2022.